Supramolecular Spintronic Devices: Spin Transitions and Magnetostructural Correlations in $[Fe_4^{II}L_4]^{8+}$ [2 × 2]-Grid-Type Complexes

Mario Ruben,[a, b] Esther Breuning,[a] Jean-Marie Lehn,*[a] Vadim Ksenofontov,[c] Franz Renz,[c] Philip Gütlich,*[c] and Gavin B. M. Vaughan[d]

Abstract: The magnetism of a series of tetranuclear complexes of the $[Fe^{II}_4L_4](X)_8$ [2 × 2]-grid-type was investigated, revealing the occurrence of spin transition behavior within this class of compounds. The phenomenon depends directly on the nature of the substituent R^1 in the 2-position on the central pyrimidine group of the ligand L. All Fe^{II} ions in compounds with R^1 substituents favoring strong ligand fields (R^1 = H; OH) remain completely in the diamagnetic low-spin state. Only complexes bearing R^1 substituents attenuating the ligand field by steric (and to a lesser extent electronic) effects (R^1 = Me; Ph) exhibit spin transition behavior triggered by temperature. In general, gradual and incomplete transitions without hysteresis were observed for magnetically active complexes. The systems described provide approaches to the development of (supra)molecular spintronics.

Keywords: iron · magnetic susceptibility · Mössbauer spectroscopy · N ligands · spin transition · supramolecular chemistry

Introduction

The next frontier in data storage, just before entering the realm of the quantum effects, lies in the nanodomain of the molecule. Molecular systems, which are capable of undergoing externally triggered transitions between two or more different states have attracted increasing interest during the last decades in view of their potential for future applications.[1] Such bi- or multistability at the molecular level, as required for high density information storage devices, might be achieved by exploitation of changes in intrinsic molecular properties, such as conformational, spin, magnetic, electronic, or photophysical states. Among the feasible effects, the spin transition (ST) phenomenon of Fe^{II} ions is one of the perspective processes to enable molecular memory effects due to the concomitance of possible "write" (temperature, pressure, light) and "read" (magnetic, optical) parameters.[2a] Such features provide access to the development of (supra)-molecular spintronics.[3]

So far, predominantly mononuclear[2] and only some binuclear,[4a] one trinuclear,[4b] and one pseudo-pentanuclear[4c] molecular Fe^{II} spin transition compounds have been investigated. Most investigations have concerned the influence of weak intermolecular interactions (hydrogen bonding; π – π stacking) on the cooperativity of the spin transition processes in the solid state. On the other hand, polymeric Fe^{II} compounds involving 1,2,4-triazole and 1,2,3,4-tetrazole ligands have been subject of several investigations.[5]

In a previous communication, a [2 × 2] grid-type Fe_4^{II} complex (**4** herein) was described as the first tetranuclear compound exhibiting ST properties,[6] generated by a consequent application of self-assembly on ST systems.

Self-assembly processes open the way to generate functional supramolecular devices by spontaneous, but controlled buildup from their components.[7] Such self-fabrication techniques are of particular interest, due to the possibility of bypassing tedious nanofabrication and nanomanipulation procedures.[8]

Furthermore, previous publications reported on particular magnetic and electrochemical properties of analogous $[Co_4^{II}L_4]^{8+}$ [2 × 2] grid species.[9, 10]

[a] Prof. Dr. J.-M. Lehn, Dr. M. Ruben, Dr. E. Breuning
ISIS-ULP-CNRS UMR-7006
8 Allée Gaspard Monge, B.P. 70028, 67083 Strasbourg Cedex (France)
Fax: (+33) 3-90-24-51-40
E-mail: lehn@isis.u-strasbg.fr

[b] Dr. M. Ruben
Present address: Institut für Nanotechnologie
Forschungszentrum Karlsruhe GmbH
P.F. 3640, 76021 Karlsruhe (Germany)

[c] Prof. Dr. P. Gütlich, Dr. V. Ksenofontov, Dr. F. Renz
Institut für Anorganische Chemie und Analytische Chemie
Johannes Gutenberg-Universität Mainz
Staudingerweg 9, 55099 Mainz (Germany)

[d] Dr. G. B. M. Vaughan
European Synchrotron Radiation Facility (ESRF)
Beamline 11
B.P. 220, 38043 Grenoble Cedex (France)

DOI: 10.1002/chem.200304933

Since self-assembled tetranuclear $[Fe_4^{II}L_4]^{8+}$ [2 × 2] grid-type species appeared to be a promising new class of ST compounds, a series of complexes $[Fe_4^{II}L_4](X)_8$ **1**–**8** (L = **A**–**H**; X = PF_6^-, BF_4^- or ClO_4^-; see Scheme 1) was synthesized and their ST properties were studied both in solution and in the solid state. ^{1}H NMR and UV/Vis techniques were used in solution, while magnetic susceptibility, X-ray diffraction and Mössbauer investigations were carried out in the solid state to reveal the influence of the nature of ligand L on the magnetic behavior of the complexes.

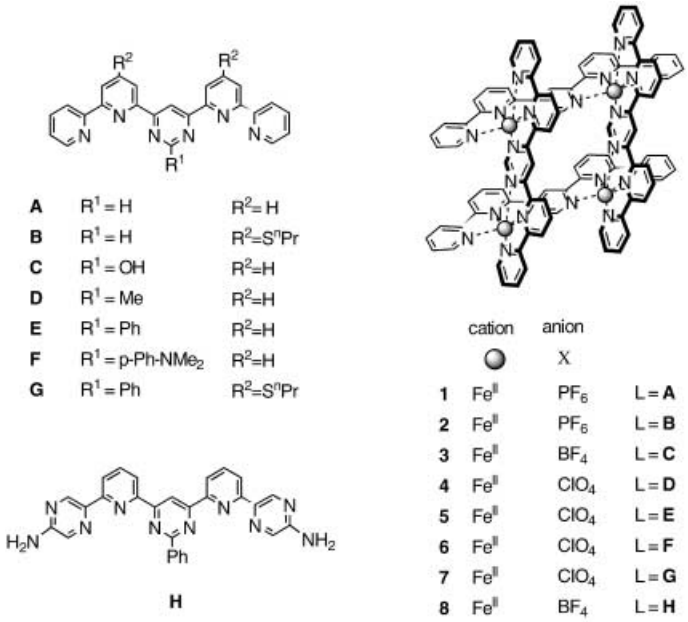

Scheme 1. Ligands **A**–**H** and [2 × 2] grid complexes **1**–**8.**

In a first series of compounds (compounds **1**–**5** $[Fe_4^{II}L_4](X)_8$), the coordination sphere of the [2 × 2] grid-type complexes was varied by changing the substituent R^1 in the 2-position of the pyrimidine of the incorporated ligands L (L = **A**–**E** with R^1 = H, OH, Me, Ph, *p*-PhNMe$_2$). In the second series of compounds, the ligands were additionally altered at the periphery. In complexes **6** and **7** S-*n*-propyl groups were introduced in the 4′-position of the ligands (complex **6** $[Fe_4^{II}\mathbf{F}_4](PF_6)_8$;[11] and complex **7** $[Fe_4^{II}\mathbf{G}_4](ClO_4)_8$). In complex **8**, $[Fe_4^{II}\mathbf{H}_4](BF_4)_8$, the peripheral pyridyl ring of the ligand backbone was exchanged by a 5″-aminopyrazin-2″yl group yielding ligand **H** (Scheme 1).

Abstract in French: *Une série de complexes **1**–**8** de type grille [2 × 2], $[Fe^{II}_4L_4](X)_8$, a été synthétisée et leurs propriétés magnétiques ont été étudiées, révélant des phénomènes de transition de spin pour les ions Fe^{II} dans ces complexes. Ce comportement est directement dépendant de la nature du substituent R^1 en position 2 sur le noyau pyrimidine du ligand L. Tous les composés avec un substituent R^1 donnant champ de ligand fort (R^1 = H, OH) restent complètement dans l'état de spin bas. Les complexes n'ayant que de substituents qui affaiblissent le champ de ligand par des effets stériques (ou dans une moindre mesure électroniques) (R^1 = Me, Ph) montrent une transition de spin induite par la température. Généralement, des transitions très graduelles et incomplètes ne présentant aucune hystérésis, ont été observées pour les composés magnétiquement actifs. Les systèmes décrits représentent une voie d'accès au développement d'une spintronique moléculaire.*

Results

Synthesis: The synthesis of the ligands has been described elsewhere (see Experimental Section). The $[Fe_4^{II}L_4]^{8+}$ [2 × 2] grid-type complexes **1**–**8** (Scheme 1) were generated by self-assembly from the corresponding metal salt and ligand in acetonitrile or methanol solution. For the complexes **1, 2**, and **6**[11] even rather long reaction times (2–3 days under reflux, in the case of **2** under deprotonation of ligand **B**) do not drive the self-assembly process to completion. Therefore, in these cases, further purification steps became necessary (**1**, **6**: column chromatography; **2**: recrystallization) and delivered the pure compounds in modest yields (**1:** 8 %; **2**: 23 %; **6:** 18 %[11]). On the other hand, the self-assembly of complexes **3**–**5, 7**, and **8** was accomplished after only 2–6 h at room temperature giving quantitative yields without further purification. In these cases, the crude products showed correct analytical data and were directly used in the subsequent investigations.

^{1}H NMR spectroscopic analysis: At room temperature, solutions of Fe_4^{II} complexes **1, 2**, and **6** give rise to the usual diamagnetic ^{1}H NMR spectra with typical shifts between $\delta = 0$ and 10 ppm. All other complexes (**3**—**5, 7**, and **8**) exhibit shifts over a wide range, between $\delta = -20$ and +150 ppm (so-called paramagnetically shifted spectra). Characteristic spectra for both cases are depicted in Figure 1 for complexes **1** and **3**. The number of signals observed coincides in all cases with the expected number of signals of the respective, symmetrically coordinated, ligands. No coupling patterns have been observed for the paramagnetic shifted peaks.

On the stepwise decrease of the temperature of the solutions of complexes exhibiting paramagnetic behavior, new peaks between $\delta = 0$ and 10 ppm emerge at the expense of the paramagnetically shifted peaks finally reaching an almost completely diamagnetic situation at low temperatures (228 K). Temperature-dependent ^{1}H spectra of complex **4** $[Fe_4^{II}\mathbf{D}_4](ClO_4)_8$ were described earlier in a temperature range from 308 K to 228 K.[6]

UV/Vis spectroscopy: The absorption spectra of compounds **1**–**8** in acetonitrile show two strong absorption bands in the UV region and, in addition, several weak and broad absorption bands in the visible region (Figure 2). However, the most remarkable feature is that all compounds with a R^1 = H or OH (**1**, **2**, and **6**) exhibit absorption bands in the visible range with absorption coefficients $\varepsilon = 2.5-3.5 \times 10^4\,\text{M}^{-1}\,\text{cm}^{-1}$ superior to those of complexes with R^1 = Me, Ph, or *p*-Ph-NMe$_2$ (**3**–**5**, **7**, and **8**, with $\varepsilon = 0.5-1.8 \times 10^4\,\text{M}^{-1}\,\text{cm}^{-1}$) at room temperature.

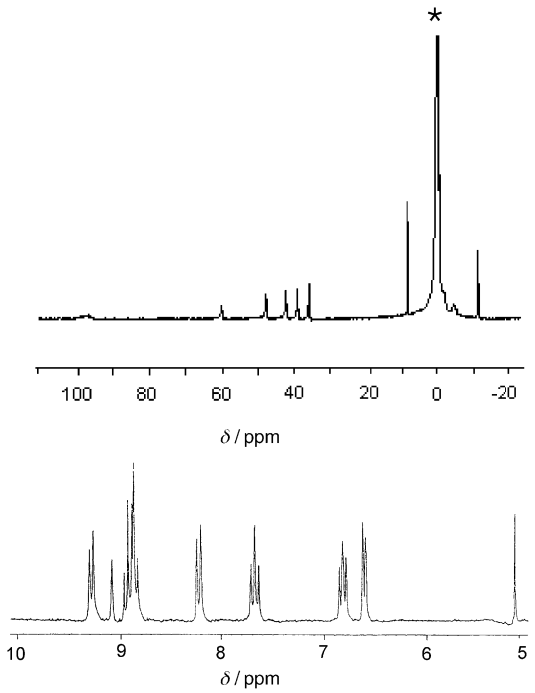

Figure 1. ^{1}H NMR spectra in CD_3CN of complex **1** (bottom) and of complex **3** (top, the asterisk marks the solvent signal).

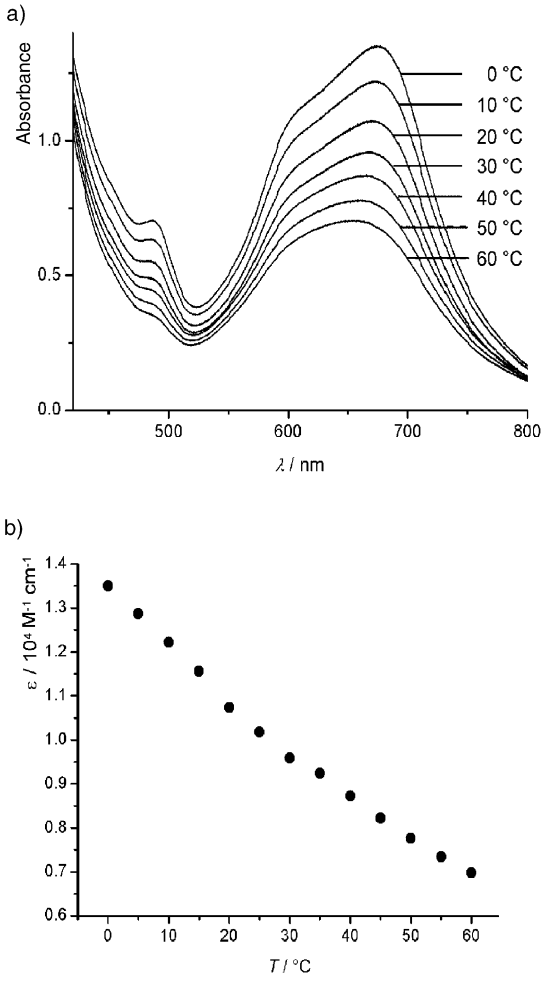

Figure 2. a) UV/Vis spectra of complex **4** in acetonitrile between 0 °C and 60 °C; b) extinction coefficient ε as a function of the temperature.

Increasing the temperature of the solutions of complexes **3**–**5** and **7** and **8** in acetonitrile resulted in a strong decrease of the corresponding absorption band, while the intensity remained completely unchanged for compounds **1**, **2**, and **6**. As an example, Figure 2 depicts the temperature-dependent behavior of complex **4**, $[Fe_4^{II}\mathbf{D}_4](ClO_4)_8$, for which an almost linear change in intensity with temperature is observed in the range between 273 and 333 K.

Single-crystal X-ray investigations: Crystals of compound **7**, $[Fe_4^{II}\mathbf{G}_4](ClO_4)_8$, were grown by diffusion of diisopropyl ether into a solution of the complex in acetonitrile. The structure of **7** was determined at 120 K and yielded a monoclinic space group $P2_1/c$. It was not possible, however, to use the same crystal for data collection at 298 K, apparently due to a phase transition.

The investigation reveals a tetranuclear complex with four inequivalent Fe^{II} ions in a pseudo-octahedral N_6 environment. The ligands are found in an almost ideal alignment in perpendicular and parallel directions (Figure 3). The distance between the pyrimidine rings of two parallel ligands averages 7.0 Å, whereby the peripheral pyridine rings of the ligands are slightly bent inside. The substituents R^1 are perpendicularly twisted with respect to the pyrimidine rings and are sandwiched between the two opposite ligands in a distance of $d =$ 3.5 Å. This distance is an argument for an effective π-stacking between the respective pyridine groups of the ligands and the $R^1 =$ phenyl substituents.

All Fe–N bond lengths are different at each Fe^{II} ion, generally exhibiting longer bond lengths to the less basic pyrimidine nitrogen atoms than to the pyridine nitrogen sites. The internal pyridine nitrogen atoms present slightly shorter bonds than their peripheral equivalents. These differences in bond lengths result in an overall axial distortion of the coordination N_6 octahedron ($\Delta_{ax} \approx -0.1$ Å).

The single X-ray investigation of $[Fe_4^{II}\mathbf{D}_4](ClO_4)_8$ (**4**) was reported previously for temperatures of 100 K and 298 K.[6] The same space group, $P\bar{1}$, was retained at both temperatures; no crystallographic phase transition was observed. Complex **4** presented at both temperatures structural features similar to those obtained for complex **7** (rectangular shape, sandwiched phenyl substituent, π-stacking).

The average Fe–N bond lengths of **7** at 120 K show that two of the Fe^{II} ions have distances of about $d = 2.15$ and 2.16 Å, while the other two are considerably shorter ($d = 2.07$ and 1.99 Å, Table 1).

In comparison, the average Fe–N bond lengths of **4**[6] present the following picture. At low temperature, three Fe^{II} ions exhibit shorter bond lengths of $d = 1.99$–2.01 Å, while the fourth remains at a longer distance of $d = 2.20$ Å. Increasing the temperature of complex **4** to room temperature reverses the situation: three of the Fe^{II} ions exhibit now longer distances of $d = 2.17$–2.19 Å, while the fourth remains with a short bond distance of $d = 2.07$ Å.

Magnetic susceptibility measurements: Complexes **1**, **2**, and **6** remain diamagnetic over the whole temperature range between 4 K and 300 K, while for the other complexes investigated, the magnetic moments change with the temper-

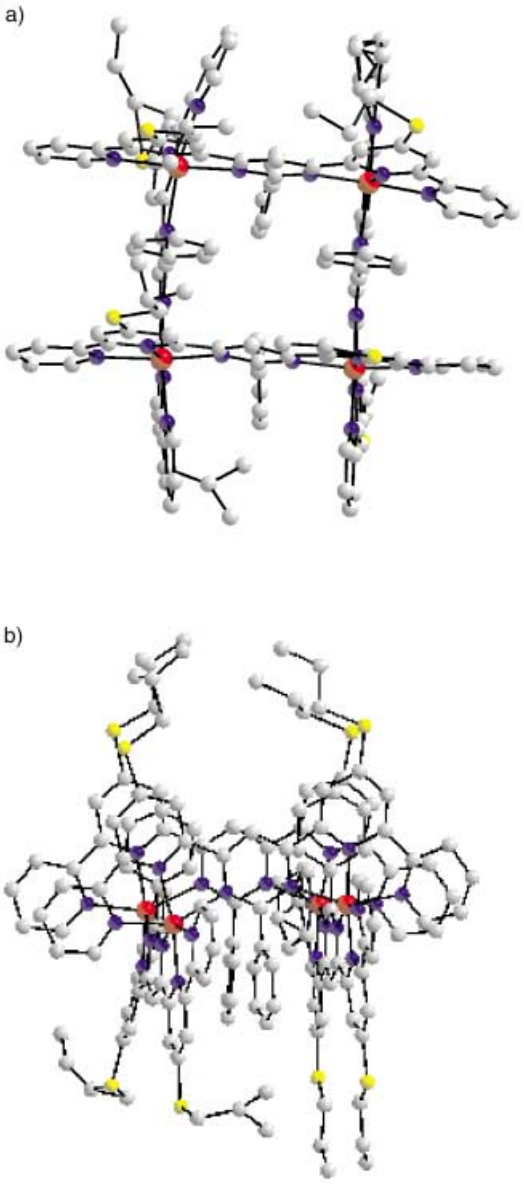

Figure 3. Top (a) and side view (b) of the single-crystal X-ray investigation of complex **7;** some of the S-*n*-propyl chains are disordered (anions, solvent molecules, and hydrogen atoms are omitted for clarity).

ature. The magnetic properties of two series of these complexes are represented in Figure 4 and 5 in the form of $\chi_M T/4$ versus T plots. $\chi_M T/4$ refers to the molar magnetic susceptibility (χ_M) times temperature (T) normalized to one Fe^{II} ion and corrected for diamagnetic contributions, $\chi_D = -357.8 \times 10^6\ cm^3 mol^{-1}$ using Pascal's constants.[12]

All magnetic plots present gradual slopes without hysteresis loops. Another common feature is the strong drop of the $\chi_M T/4$ values for all magnetic curves below 30 K.

In the first series of complexes **3**–**5**, the substituent R^1 was varied from methyl via phenyl to *para*-dimethylaminophenyl. This results in similar plot shapes but different maxima of the susceptibility at room temperature (Figure 4).

Table 1. Average Fe–N bond lengths in Å for the perchlorate salts of **4** (at 173 K and 293 K) and of **7** (at 120 K).

	4[6] 293 K	**4**[6] 173 K	**7** 120 K
Fe1–N	2.19	2.20	2.164(5)
Fe2–N	2.17	2.01	2.148(5)
Fe3–N	2.07	1.99	2.067(6)
Fe4–N	2.17	2.01	1.986(6)

In a second series of the complexes **4**, **7**, and **8** the pyrimidine substituent was maintained ($R^1 = Ph$), while the peripheral substitution pattern (**4**: $R^2 = H$; **7**: $R^2 = S^nPr$; **8**: introduction of a 5″-aminopyrazin-2″yl ring) was varied. The ligand variations modified the shapes of the magnetic susceptibilities versus temperature plots, while the maxima at room temperature remained relatively unchanged (Figure 5).

Mössbauer spectroscopy: The Mössbauer effect, a microscopic tool, was used to probe the spin states and oxidation states of the metal ions.[13] Complex **6**, $[Fe_4^{II}\mathbf{F}_4](PF_6)_8$, exhibits a doublet with an isomer shift $\delta = 0.178$ (0.093) mm s^{-1} (relative to Fe/Rh) and a quadrupole splitting of 1.197 (1.173) mm s^{-1} shown at 4.2 K (300 K), which remains constant over all the temperature range from 10 K to 300 K (Figure 6a). An additional small signal arises at 330 K from an impurity in the detector window (10% at 300 K).

The same investigation using complex **4**, $[Fe_4^{II}\mathbf{D}_4](ClO_4)_8$, resulted in the observation of two doublets at 4.2 K: one with an isomer shift $\delta = 0.402(6)$ mm s^{-1} and a quadrupole splitting of 1.37(1) mm s^{-1}, and a second with an isomer shift of $\delta =$ 1.090(8) mm s^{-1} and a quadrupole splitting of 2.17(1) mm s^{-1} (Figure 6b). Taking equal Lamb–Mössbauer factors for both signals, the area fraction of these signals is 54 and 46%, respectively. Upon increasing the temperature, the first doublet loses intensity in favor of the second doublet, yielding

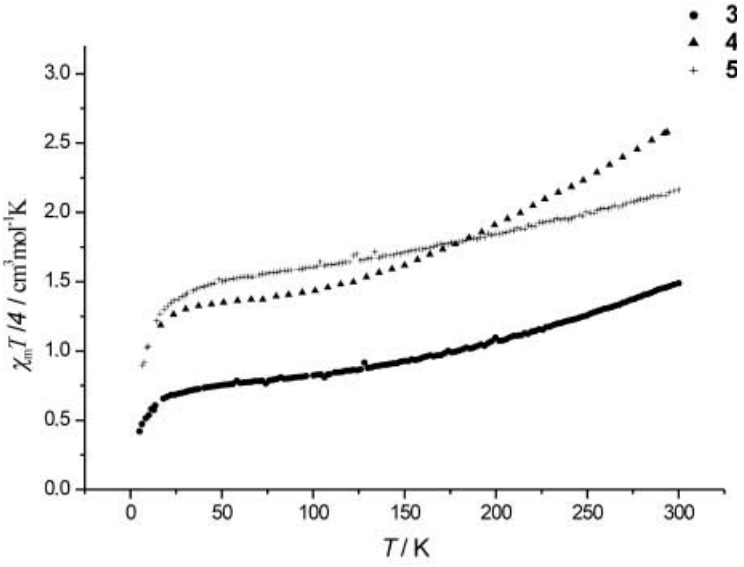

Figure 4. $\chi_M T/4$ versus T plots of complexes **3**–**5**: Influence of the variation of the substituent R^1 (R^1 = Me, Ph, *p*-PhNMe$_2$) on the magnetism.

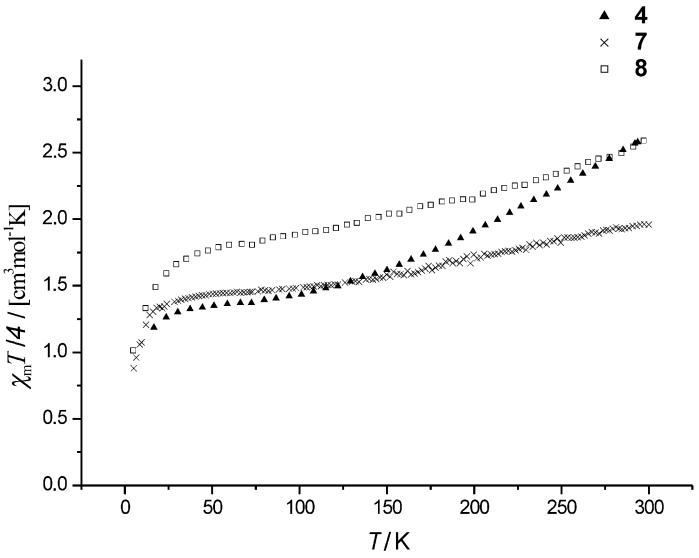

Figure 5. $\chi_M T/4$ versus T plots of complexes **4**, **7**, and **8**: Variation of the peripheral substituents of the ligands (maintaining substituent $R^1 = Ph$).

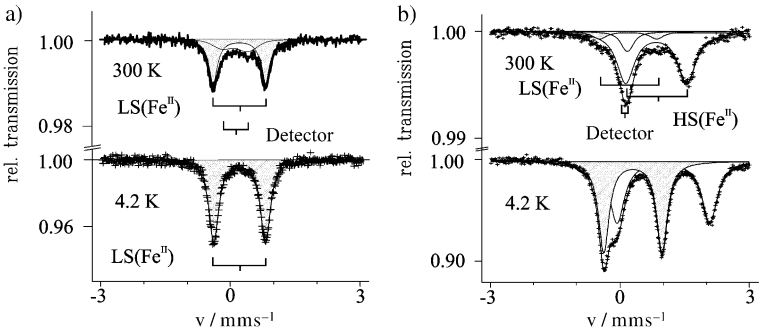

Figure 6. Mössbauer spectra of a) **6** and b) **4** at various temperatures.

a 10 to 80% ratio at 300 K. As also found for **6**, above 193 K an additional small signal emerges due to impurity in the detector window (10% at 300 K).

Discussion

The characteristics observed during the self-assembly process subdivide the complexes **1**–**8** into two classes of compounds. All complexes with $R^1 = H$ or OH (**1**, **2**, and **6**) show slow formation kinetics and result in low yields. In contrast, all complexes with $R^1 = Me$, Ph, or *p*-$PhNMe_2$ undergo self-assembly in a short time with quantitative yields of the respective products **3**–**5**, **7**, and **8**. Clearly, the substituent R^1 close to the coordinating pyrimidine nitrogen donor atoms plays a predominant role in the kinetics of the self-assembly process, while changes in other, more peripheral, ligand positions influence the reaction parameters to a much lesser extent.

As known from other Fe^{II}–ligand systems, the introduction of sterically demanding substituents in the neighboring position of a coordinating nitrogen provokes the (partial) transition of Fe^{II} ions from the low-spin ground state into the high-spin state (vide infra).[14, 15] The differences in reaction times and yields of the self-assembly processes may be related to the fact that the kinetics of ligand exchange of Fe^{II} ions in the low-spin (LS; $t_{2g}^6\ e_g^0$) and high-spin (HS; $t_{2g}^4\ e_g^2$) state differ markedly. Similar observations were reported on Fe^{II} ions in the gas phase, but have not yet been described for Fe^{II} ions in solution.[16] It is known from ligand field theory, that the "closed shell" Fe^{II}(LS) state is kinetically more inert than the "open shell" HS state, thus leading to slower ligand exchange. As reversibility of the bond formation is essential for the self-assembly process, the formation of the final $[2 \times 2]$ grid structure is inhibited, resulting in slow and incomplete reactions. The introduction of bulky R^1 substituents results in an "open shell" HS configuration at reaction temperature by attenuation of the ligand field and thus drives the self-assembly process to completion in much shorter times.

All ^{1}H NMR spectra illustrate the formation of highly symmetric structures in agreement with the proposed $[2 \times 2]$ grid-like motif. The number of signals, in combination with the composition of the complexes obtained by mass spectroscopy, elemental analysis and X-ray investigations, allows the unambiguous assignment of the $[2 \times 2]$ grid-type nature for both dia- and paramagnetic complexes.

Figure 1 illustrates the effect of incorporation of Fe^{II}(LS) or Fe^{II}(HS) ions on the room-temperature ^{1}H NMR spectra: all complexes (**1**, **2**, and **6**) with Fe^{II}(LS) ions exhibit only signals in a region expected for diamagnetic complexes ($\delta = 0-10$ ppm). In contrast, those of the paramagnetic complexes (**3**–**5**, **7**, and **8**), show peaks spread across a wide range ($\delta = -20-180$ ppm). The strong shift of peaks in the proton NMR spectra is caused by the high local field typical for paramagnetic Fe^{II}(HS) ions.[17] Furthermore, the absence of coupling patterns can be attributed to broadening by increased relaxation rates near the strong polar fields of the Fe^{II}(HS) ions. Because of these two features, non-diagnostic shifts and absence of any coupling patterns, an assignment of the peaks was only achieved for some of the signals by cross comparison of the differently substituted complexes **3**–**5, 7**, and **8**, however, not conclusively and completely for all signals.

Temperature-dependent ^{1}H NMR investigations confirmed the proposed spin transition behavior of paramagnetically shifted complexes in solution.[6] Upon stepwise cooling from 308 to 208 K, the paramagnetically shifted peaks are first broadened, later disappearing in favor of new signals found in the "diamagnetic" region of the spectrum. This process was proven to be completely reversible. Thus, in solution the course of the spin transition can be described by a Boltzmann approach with a temperature-dependent distribution over the HS and LS states.

The room-temperature electronic spectra of all compounds **1**–**8** show qualitatively similar features with two main transitions bands in the UV and two in the visible region. The two transitions in the UV region can be attributed to ligand-centered $\pi-\pi^*$ transitions of the pyridine and the pyrimidine groups. In the visible region, the two distinct maxima coincide with the Fe^{II}(LS)–pyridine MLCT band, as

also observed in $[Fe(tpy)_2](PF_6)_2$ ($\lambda_{max} = 518$ nm).[18] The Fe^{II}(LS)–pyrimidine MLCT transition is found at significantly longer wavelengths, since the pyrimidine LUMO is of lower energy than the pyridine LUMO, such that the respective MLCT has a smaller band gap.

The subdivision of the investigated compounds into dia- and paramagnetic compounds is also mirrored by the absorption coefficients derived from the MLCT bands. All diamagnetic complexes (**1**, **2**, and **6**) show values close to the sum of those of four mononuclear $[Fe(tpy)_2]^{2+}$ segments ($\varepsilon = 9200\,M^{-1}cm^{-1}$).[18] In contrast, all paramagnetic compounds exhibit dramatically decreased absorption coefficients at room temperature. This can be explained by the involvement of occupied antibonding e* orbitals in the Fe^{II}(HS) state, which leads to elongated Fe–N bonds and reduced overlap integrals and consequently to very weak or undetectable MLCTs under standard conditions.[19] Evidently, the observed intensities of the MLCT bands originate almost exclusively from Fe^{II}(LS) to ligand transitions. Thus, the comparison of the absorption coefficients of dia- and paramagnetic complexes gives already a first rough estimate of the ratio of Fe^{II}(LS) and (HS) ions at room temperature in solution.

In addition, as shown for compound **4** in Figure 2, the absorption coefficients of the paramagnetic complexes decrease almost linearly with increasing temperature, thus indicating the transformation of visible light-absorbing Fe^{II}(LS) ions into "colorless" Fe^{II}(HS) ions.

The X-ray investigations of both complexes **4**[6] and **7**, show pseudooctahedral N_6 surroundings for all Fe^{II} ions. All four ions are crystallographically inequivalent in each structure and exhibit very different Fe–N bond lengths. The Fe–N bond lengths do not only vary considerably between the four Fe^{II} ions within one complex, but also for the respective six bonds around each of the four coordination centers. These deviations are due to the differences in π-basicity of the pyridine and of the pyrimidine nitrogen atoms on the one hand and due to small distortions originating from the electronic structure of the d^6 HS systems on the other hand.[20]

The average Fe–N bond lengths can be used as an indicator for the spin state, since the population of the antibonding e_g* orbitals in the HS case causes an elongation of the bond length by about 0.2 Å.[21] Thus, at 100 K in complex **4** three of the four metal ions show bond lengths close to those characteristic of the Fe^{II}(LS) state, while the fourth remains at bond lengths typically observed for the Fe^{II}(HS) state.[6] Following the same argumentation, we can conclude that complex **7** presents at 120 K a situation pointing to two HS and one LS Fe^{II} sites with a last one in between (d(Fe–N) = 2.06 Å). The latter can be interpreted by the occurrence of disorder over the sites within the averaging of the bond lengths over the coherence wavelength.

At 298 K, the crystal structure of **4** indicates that three of the Fe^{II} ions are in a HS situation, while the fourth exhibits once more a bond length apparently between the LS and HS state.[6] The differences in the average bond lengths in **4** and **7** at low temperatures as well as the bond length change on increasing the temperature in **4** indicate clearly a spin transition behavior of the paramagnetic complexes in the solid state.

The solid-state magnetic properties of the present complexes were examined directly by magnetic susceptibility measurements. The paramagnetic complexes **3**–**5**, **7**, and **8** were studied in two different ligand variation series, while the compounds **1**, **2**, and **6** are diamagnetic. In general, all paramagnetic complexes present very gradual and incomplete spin transitions with a sharp decrease of the magnetic moment below 30 K due to the zero-field splitting of the Fe^{II}(HS) ion.[22] No hysteresis was detected, which is in line with the very gradual spin transition apparently arising from very weak cooperative interactions.[2]

In the first series **3**–**5**, the substitution of R^1 resulted in very similarly shaped magnetic curves, but with different maximum values of susceptibilities $\chi_M T/4$ at room temperature. In the case of compound **3** (R = methyl) a value of $\chi_M T/4 = 1.5\,cm^3\,K\,mol^{-1}$ indicates a magnetic situation close to the presence of 2LS/2HS in one molecule, while compounds **4** and **5** exhibit room temperature $\chi_M T$ *values* closer to a 1LS/3HS situation ($\chi_M T/4 = 1.9$ and $2.5\,cm^3\,K\,mol^{-1}$).

The second series (**4**, **7**, and **8**), where R^1 = phenyl is conserved but the peripheral ligand sphere varies, yields slightly higher $\chi_M T$ values at room temperature (close to a 1LS/3HS situation for **4** and **8** and a 2LS/2HS for **7**), but shows clear differences in the change of $\chi_M T$ with temperature. Complex **8**, which may undergo intermolecular hydrogen-bonding interactions, shows the biggest $\chi_M T$ values and the smallest slope of all investigated compounds within the temperature range studied. On the contrary, compound **4** displays a more structured progression, while complex **7** presents a pronounced magnetic plateau up to 150 K and a small, but continuous slope at temperatures above 150 K. However, the highest experimental $\chi_M T$ values in both series remain below the theoretical spin-only value of a Fe^{II} ion in the high spin state ($\chi_M T/4 = 3.2\,cm^3\,K\,mol^{-1}$).

The Mössbauer spectra were investigated for one diamagnetic and one paramagnetic compound as typical examples. Compound **6** shows a doublet of Fe^{II}(LS) at all temperatures investigated. On the other hand, compound **4** presents two doublets at $T = 4.2$ K with characteristics typical for Fe^{II}(LS) (small isomeric shift and small quadrupole splitting) and Fe^{II}(HS) (large isomeric shift and large quadrupole splitting) under the given symmetric environments. The low-temperature spectrum accounts for a 3LS/1HS situation, while at high temperature the reverse situation is observed. This confirms once more a thermally induced spin transition for the paramagnetic compounds.

Conclusion

The occurrence of spin transition in [2 × 2] grid-like complexes of the type $[Fe^{II}_4\mathbf{L}_4](A)_8$ depends directly on the nature of the substituent R^1 in the 2-position of the ligand L. All compounds with substituents in this position favoring strong ligand fields (R^1 = H; OH) remain completely in the LS state at all temperatures studied. Only complexes bearing substituents which attenuate the ligand field by steric (and to lesser extent electronic) effects (R^1 = Me; Ph), exhibit, although incomplete, temperature triggered spin transition.

The magnetic behavior was characterized in solution by ^{1}H NMR and UV/Vis spectroscopy and in the solid state by X-ray, magnetic susceptibility, and Mössbauer measurements. Very gradual and incomplete transitions without hysteresis seem to be typical for all investigated, magnetically active compounds of the $[Fe^{II}_4\mathbf{L}_4](X)_8$ [2 × 2] grid-type. The presence of the substituent $R^1 = Ph$ resulted in the most complete transition and further substitutions at the phenyl ring or in the 4′-position of the ligand altered the spin transition behavior only marginally. Improving the intermolecular interaction between the tetranuclear centers by introduction of hydrogen bonding between the grid units increased the HS fraction over the whole temperature range, although the spin transition remained very gradual and incomplete.

The question of cooperativity within and between the molecular building blocks is being investigated. Moreover, further work is being directed toward the construction of larger functional architectures using grid-like building blocks in extended hierarchic self-assembly processes.

In a farther-reaching perspective, architectures presenting spin state properties that may be switched by external triggers represent entries toward (supra)molecular spintronics.[3]

Experimental Section

Magnetic measurements: The magnetic measurements were carried out with a Foner susceptometer and a SQUID Magnetometer (Quantum Design) working in the 4.2 – 300 K temperature range. The applied magnetic field was 1 T.

Mössbauer spectra: Mössbauer spectra were recorded in transmission geometry with a Co/Rh source kept at room temperature and a conventional spectrometer operating in the constant-acceleration mode. The samples were sealed in a plexiglass sample holder and mounted in a helium-bath cryostat for temperature variation between 4.2 and 300 K. The spectra were fitted to Lorentzian-shaped lines using a nonlinear iterative minimisation routine (MOSFUN).

X-ray structural analysis of complex 7: A suitable pine-green prism (0.02 × 0.02 × 0.04 mm) of $[C_{144}H_{128}N_{24}S_8Fe_4]^{8+} \cdot 8ClO_4^- \cdot 3CH_3CN \cdot 5H_2O$ was obtained from acetonitrile – diisopropyl ether. The data were recorded at 120.0(2) K on Beamline ID11 at the ESRF. Phi rotation images (1 s per frame) were recorded with a Bruker Smart 6500 camera and a Si(111) monochromated wavelength of 0.45085 Å. The data were integrated with the Bruker data reduction suite Saint and the absorption correction applied via SADABS. Structure solution was performed by direct methods (SHELXS)[23] and refinement against F^2 (SHELXL).[24] The hydrogen atoms were calculated to their idealized positions with isotropic temperature factors (1.2 or 1.5 times the C temperature factor) and were refined as riding atoms. Due to the poor diffracting power of the crystal and the consequent low number of strong observations, geometric constraints were applied in order to keep the data/parameter ratio acceptable. Many of the thiol side chains and one of the perchlorate ions were disordered between different sites.

Complex 7: (at 120 K) monoclinic, $P2_1/c$, $a = 26.266(2)$, $b = 19.930(2)$, $c = 33.801(4)$ Å, $\beta = 110.378(5)^\circ$, $V = 16587(3)$ Å^3, $Z = 4$, $\rho_{calcd} = 1.344$ g cm^{-3}, $2\theta_{max} = 22.4^\circ$, $\mu(0.45085\ Å) = 0.317$ mm^{-1}. A total of 38325 collected reflections, 10188 unique reflections [5838 with $I > 2\sigma(I)$] were used for refinement. The final R values were $R = 0.121$, $wR^2 = 0.325$ [$I > 2\sigma(I)$], $R = 0.187$, $wR^2 = 0.364$ (all data) for 1294 parameters and 2249 restraints. The highest electron density on the final difference map was 0.671 e Å^{-3}.
CCDC-205093 contains the supplementary crystallographic data for this paper. These data can be obtained free of charge via www.ccdc.cam.ac.uk/conts/retrieving.html (or from the Cambridge Crystallographic Data Centre, 12 Union Road, Cambridge CB2 1EZ, UK; fax: (+44) 1223-336033; or deposit@ccdc.cam.uk).

Synthesis

General: All reagents were obtained from commercial suppliers and used without further purification unless otherwise noted. The following solvents were distilled prior to use: tetrahydrofuran (THF) and diethyl ether from sodium and benzophenone, and dimethyl sulfoxide (DMSO) from calcium hydride under argon. All organic solutions were routinely dried over magnesium sulfate or sodium sulfate and solvents were removed under vacuum using a rotary evaporator. ^{1}H and ^{13}C NMR spectra were recorded on a Bruker AC 200 spectrometer at 200 MHz and 50 MHz, respectively. Flash chromatography was performed using neutral alumina (activity 2). FAB mass spectra were performed on a Fisons TRIO-2000 (Manchester) and a Micromass AUTOSPEC-M-HF spectrometer using 3-nitrobenzylic alcohol as matrix. Microanalyses were carried out by the Service de Microanalyse, Faculté de Chimie, Strasbourg. Melting points were measured on a digital electrothermal apparatus and are uncorrected.

Ligands: The synthesis of ligands **A**,[25] **C**,[26] **D**,[27] **E**,[27] **F**,[11] **G**, [10b] and **H**[28] is described elsewhere. Ligand **B** was synthesized by using Stille-type coupling procedures following the reactions depicted in Scheme 2.

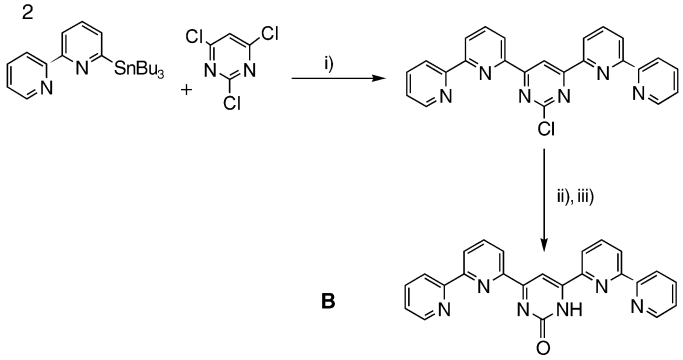

Scheme 2. Reaction scheme for the synthesis of ligand **B:** i) $[Pd(PPh_3)_4]$ (cat.), toluene; ii) NaOBn, BnOH; iii) excess CF_3SO_3H, toluene.

6-(Tributylstannyl)2,2′-bipyridine[26](970 mg, 2.1 mmol), 2,4,6,-trichloropyrimidine (200 mg, 1.09 mmol), and $[Pd(PPh_3)_4]$ (153 mg, 0.22 mmol) were combined in DMF (5 mL), flushed with argon, and heated under reflux for 48 h. The solvent was evaporated and the resulting brown crude material was washed with methanol several times. The product 4,6-bis(2′,2″-bipyrid-6′-yl)-2-chloropyrimidine remained as a white powder in 60 % yield (270 mg, 0.65 mmol).

4,6-Bis(2′,2″-bipyrid-6′-yl)-2-chloropyrimidine (85 mg, 0.2 mmol) was suspended in benzylic alcohol (30 mL), and NaOBn (0.28 mL, 1 M in methanol) was slowly added. The suspension was heated at 120 °C until all solid had disappeared resulting in a dark yellow solution. The solvent was removed in vacuo and the remaining crude product dissolved in toluene. This solution was treated with an excess of triflic acid (10 mL) under reflux for 2 h. The resulting solid was filtered and suspended three times in *n*-hexane (10 mL) immersing it each time into a ultrasound bath for about five minutes. The remaining solid was recrystallized twice from methanol yielding 45 mg of a white powder (0.11 mmol, 55 %).

Ligand C: 4,6-bis(2′,2″-bipyrid-6′-yl)-pyrimid-2-one: ^{1}H NMR (200 MHz, $[D_6]$DMSO, 298 K): $\delta = 8.81$ (d, $J = 5.1$ Hz, 2H), 8.74 (d, $J = 8.1$ Hz, 2H), 8.61 (d and s, $J = 7.7$ Hz 3H), 8.50 (d, $J = 6.82$ Hz, 2H), 8.23 (t, $J = 8.1$ Hz, 2H), 8.15 (t, $J = 7.66$ Hz, 2H), 7.62 (t, $J = 5.1$ Hz, 2H), 4.77 ppm (s, 1H); ^{13}C NMR: not determined due to insufficient solubility ; FAB-MS: m/z: 405.0 [M^+]; elemental analysis calcd (%) for $C_{24}H_{16}N_6O$: C 71.28, H 3.99, N 20.78; found: C 70.78, H 3.81, N 19.09.

Complexes: The synthesis of complexes **1**,[25] **4**,[8] **6**,[27] and **8**[28] was carried out following literature protocols.

Complex 2: A suspension of the ligand **B** (30 mg, 74 μmol) in anhydrous methanol (3 mL) was treated with NaOMe (74 μL of a 1 M solution in methanol). After dissolution of the ligand, the metal salt $Fe(BF_4)_2 \cdot 6H_20$ (25 mg, 74 μmol) was added and the deep blue solution was heated under reflux for 48 h. The solvent was evaporated and the remaining blue solid was recrystallized from methanol to yield complex **2** as blue, thin needles (36 mg, 17 μmol; 23 %). ^{1}H NMR (200 MHz, CD_3CN, 298 K): $\delta = 8.73$ (d, 2H), 8.46 (s and d, 3H), 8.05 (d, Hz, 2H), 7.82 (d, 2H), 7.48 (t, 2H), 6.62 (t,

2H), 6.38 ppm (t, 2H); ^{13}C NMR: (due to insolubility not possible); FAB-MS: *m/z*: 2097.1 $[M^+ - BF_4]$, 2011.1 $[M^+ - 2BF_4]$, 1924.1 $[M^+ - 3BF_4]$, 1852.1 $[M^+ - 4BF_4]$; UV/Vis (CH_3CN, nm, 298 K)(ε in $10^4\,M^{-1}cm^{-1}$): $\lambda =$ 312 (134), 383 (155), 569 (37), 694 (28), 753 (29); elemental analysis calcd (%) for $C_{96}H_{60}B_4F_{16}N_{24}O_4Fe_4 \cdot 4\,CH_3OH$: C 51.94, H 3.31, N 14.54; found: C 50.87, H 3.45, N 13.83.

Complexes 3, 5, and 7: A suspension of the ligand (19.8 μmol) and the respective Fe^{II} salt (19.8 μmol) in CH_3CN (1.5 mL) was heated shortly until the mixture was dissolved completely. The solution was stirred for 12 h at room temperature (in the case of solubility problems under reflux). The complex was isolated by evaporation of the solvent or addition of diisopropyl ether to the solution until a precipitate formed. The precipitate was collected, washed with diisopropyl ether and dried in vacuo. The crude product was used directly for the measurements without further purification.

Complex ***3***: ^{1}H NMR (200 MHz, CD_3CN, 298 K): $\delta = 140.9$, 63.1, 50.4, 44.8, 41.5, 38.4, 11.0, 8.0, −8.5 ppm; FAB-MS: *m/z*: 2430.1 $[M^+ - 2ClO_4]$, 2330.2 $[M^+ - 3ClO_4]$, 2231.4 $[M^+ - 4ClO_4]$, 2031.7 $[M^+ - 5ClO_4]$; UV/Vis (CH_3CN, nm, 298 K) (ε in $10^4\,M^{-1}cm^{-1}$): $\lambda = 274$ (95), 332(100), 346 (102), 512 (10), 585 (17), 651(5); elemental analysis calcd (%) for $C_{100}H_{72}Cl_8N_{24}O_{32}Fe_4 \cdot 5.5\,H_2O$: C 44.18, H 3.04, N 12.36; found: C 42.34, H 3.13, N 11.17.

Complex ***5***: ^{1}H NMR (200 MHz, CD_3CN, 298 K): $\delta = 141.2$, 78.0, 70.6, 64.6, 55.5, 50.3, 16.3, 7.6, 4.9, 3.7, −6.8, −17.0 ppm; FAB-MS: *m/z*: 2773.9 $[M^+ - 2BF_4]$, 2687.6 $[M^+ - 3BF_4]$, 2600.3 $[M^+ - 4BF_4]$; UV/Vis (CH_3CN, nm, 298 K) (ε in $10^4\,M^{-1}\,cm^{-1}$): $\lambda = 385$ (108), 623(13); elemental analysis calcd (%) for $C_{128}H_{100}B_8F_{32}N_{28}Fe_4 \cdot 2\,CH_3CN \cdot 6\,H_2O$: C 50.14, H 3.82, N 13.49; found: C 49.93, H 4.07, N 12.17.

Complex ***7***: ^{1}H NMR (200 MHz, CD_3CN, 298 K): $\delta = 151.9$, 77.2, 72.0, 67.0, 60.1, 54.0, 18.2, 9.0, 8.2, −0.1, −9.8; FAB-MS: *m/z*: 3370.6 $[M^+ - ClO_4]$, 3270.3 $[M^+ - 2ClO_4]$, 3171.2 $[M^+ - 3ClO_4]$, 3071.3 $[M^+ - 4ClO_4]$; UV/Vis (CH_3CN, nm, 298 K)(ε in $10^4\,M^{-1}cm^{-1}$): $\lambda = 289$ (89), 349 (110), 572 (9), 646 (7); elemental analysis calcd (%) for $C_{144}H_{128}Cl_8N_{24}O_{32}S_8Fe_4 \cdot 3\,CH_3CN \cdot 5\,H_2O$: C 48.41, H 4.06, N 10.37, S 7.03; found: C 49.43, H 4.21, N 8.61, S 7.10.

Acknowledgement

We thank Dr. D. Bassani for providing a sample of **6**. This work was supported by a post-doctoral scholarship provided by the "Deutscher Akademischer Austauschdienst" (DAAD) (M.R.). In addition, financial support from the "Ministère de l'Education Nationale de la Recherche et de la Technologie" is gratefully acknowledged (E.B.). We also thank the "Fonds der chemischen Industrie", the "Materialwissenschaftliches Zentrum" at the University of Mainz, and the European Community contract number No.: ERB-FMRX-CT98–0199 for financial help.

[1] For examples see: a) electrochemical: C. P. Collier, G. Mattersteig, E. W. Wong, Y. Luo, J. Sampaio, F. M. Raymo, J. M. Stoddart, J. R. Health, *Science* **1999**, *285*, 391–395; C. P. Collier, G. Mattersteig, E. W. Wong, Y. Luo, K. Beverly, F. M. Raymo, J. F. Stoddart, J. R. Heath, *Science* **2000**, *289*, 1172–1176; b) chiroptical: B. L. Feringa, W. F. Jager, B. de Lange, *Tetrahedron* **1993**, *49*, 8267–8310; B. L. Feringa, R. A. van Delden, N. Komura, E. M. Geertsema, *Chem. Rev.* **2000**, *100*, 1789–1816; B. L. Feringa, *Acc. Chem. Res.* **2001**, *34*, 504–513; c) photochemical: M. Irie, *Mol. Crystl. Liq. Cryst.* **1993**, *227*, 263–268; G. M. Tsivgoulis, J.-M. Lehn, *Chem. Eur. J.* **1996**, *2*, 1399–1404; S. L. Gilat, S. H. Kawai, J.-M. Lehn, *Chem. Eur. J.* **1995**, *1*, 275–284; S. H. Kawai, S. L. Gilat, R. Ponsinet, J.-M. Lehn, *Chem. Eur. J.* **1995**, *1*, 285–293; S. H. Kawai, S. L. Gilat, J.-M. Lehn, *J. Chem. Soc. Chem. Commun.* **1994**, 1011–1013; S. L. Gilat, S. H. Kawai, J.-M. Lehn, *J. Chem. Soc. Chem. Commun.* **1993**, 1439–1353.

[2] a) P. Gütlich, A. Hauser, H. Spiering, *Angew. Chem. Int. Ed. Engl.* **1994**, *33*, 2024–2054; *Angew. Chem.* **1994**, *106*, 2109–2141; P. Gütlich, A. Hauser, H. Spiering, *Spin Transition in Iron(II) Compounds , Vol. 2*, 1st ed., **1999**, Wiley, New York; O. Kahn, *Chem. Britain* **2000**, *March*, 33; P. Gütlich, Y. Garcia, H. Spiering in *Magnetism: "Molecules to Materials IV"* (Eds.: M. Drillon, J. S. Miller), Wiley-VCH, Weinheim, **2003**; b) P. Gütlich, A. Hauser, *Coord. Chem. Rev.* **1990**, *97*, 1–22; T. Buchen, P. Gütlich, K. H. Sugiyarto, H. A. Goodwin, *Chem. Eur. J.* **1996**, *2*, 1134–1138; J. F. Letard, P. Guionneau, E. Codjovi, O. Lavastre, G. Bravic, D. Chasseau, O. Kahn, *J. Am. Chem. Soc.* **1997**, *119*, 10861–10868.

[3] For spintronics in semiconductors see: S. A. Wolf, D. D. Awschalom, R. A. Buhrman, J. M. Daughton, S. von Molnár, M. L. Roukes, A. Y. Chtchelkanova, D. M. Treger, *Science*, **2001**, *294*, 1488–1495; *Semiconductor Spintronics and Quantum Computation* (Eds.: D. D. Awschalom, D. Loss, N. Samarth), Springer, **2002**.

[4] a) V. Ksenofontov, H. Spiering, S. Reiman, Y. Garcia, A. B. Gaspar, N. Moliner, J. A. Real, P. Gütlich, *Chem. Phys. Lett.* **2001**, *348*, 381–386; b) J. J. A. Kolnaar, G. van Dijk, H. Kooijman, A. L. Spek, V. G. Ksenofontov, P. Gütlich, J. G. Haasnoot, J. Reedijk, *Inorg. Chem.* **1997**, *36*, 2433–2440; c) J. J. A. Kolnaar, M. I. de Heer, H. Kooijman, A. L. Spek, G. Schmitt, V. Ksenofontov, P. Gütlich, J. G. Haasnoot, J. Reedijk, *Eur. J. Inorg. Chem.* **1999**, *5*, 881–886.

[5] L. G. Lavrenova, V. N. Ikorskii, V. A. Varnek, I. M. Oglezneva, S. V. Larionov, *Koord. Khim.* **1986**, 12, 207–212; J. Kröber, E. Codjovi, O. Kahn, F. Grolière, *J. Am. Chem. Soc.* **1993**, *115*, 9810–9812; Y. Garcia, J. Moscovici, A. Michalowicz, V. Ksenofontov, G. Levchenko, G. Bravic, D. Chasseau, P. Gütlich, *Chem. Eur. J.* **2002**, *8*, 4992–5000.

[6] E. Breuning, M. Ruben, J.-M. Lehn, F. Renz, Y. Garcia, V. Ksenofontov, P. Gütlich, E. Wegelius, K. Rissanen, *Angew. Chem.* **2000**, *112*, 4312–4315; *Angew. Chem. Int. Ed.* **2000**,*14*, 2504–2507.

[7] J.-M. Lehn, *"Supramolecular Chemistry: Concepts and Perspectives"*, VCH, Weinheim, chapters 8 and 9, **1995**; J.-M. Lehn, *Science* **2002**, *295*, 2400–2403.

[8] C. Joachim, J. K. Gimzewski, A. Aviram, *Nature* **2000**, *408*, 541–548.

[9] O. Waldmann, J. Hassmann, P. Müller, G. S. Hanan, D. Volkmer, U. S. Schubert, J.-M. Lehn, *Phys. Rev. Lett.* **1997**, *78*, 3390–3393.

[10] a) M. Ruben, E. Breuning, J.-P. Gisselbrecht, J.-M. Lehn, *Angew. Chem.* **2000**, *112*, 2563–2566; *Angew. Chem. Int. Ed.* **2000**,*39*, 4139–4142; b) M. Ruben, E. Breuning, M. Barboiu, J.-P. Gisselbrecht, J.-M. Lehn, *Chem. Eur. J.* **2003**, *9*, 291–299.

[11] D. Bassani, J.-M. Lehn, S. Serroni, F. Puntoriero, S. Campagna, unpublished results.

[12] L. N. Mulay, E. A. Boudreaux, *Theory and Applications of Molecular Diamagnetism*, Wiley-Interscience, New York, **1976**, p. 303.

[13] P. Gütlich, R. Link, A. Trautwein, "*Mössbauer Spectroscopy and Transition Metal Chemistry",* Springer, New York, **1978**.

[14] Bipyridine: D. Onggo, J. M. Hook, A. D. Rae, H. A. Goodwin, *Inorg. Chim. Acta* **1990**, *173*, 19–24.

[15] Terpyridine: E. Constable, G. Baum, E. Bill, R. Dyson, R. van Eldik, D. Fenske, S. Kaderli, D. Morris, A. Neubrand, M. Neuburger, D. R. Smith, K. Wieghardt, M. Zender, M. D. Zuberbühler, *Chem.-Eur. J.* **1999**, *4*, 498–508.

[16] D. Schröder, S. Shaik, H. Schwarz, *Acc. Chem. Res.* **2000**, *33,* 139–145.

[17] I. Bertini, C. Luchinat, *NMR of Paramagnetic Molecules in Biological Systems*, 1st ed., Benjamin/Cummings Publishing Company, Inc., Amsterdam Sydney, **1986**.

[18] P. S. Braterman, J. I. Songh, R. Peacock, *Inorg. Chem.* **1992**, *31*, 555–559.

[19] A. B. P. Lever, *Inorganic Electronic Spectroscopy*, 2nd ed., Elsevier, Amsterdam, **1984**.

[20] E. C. Constable, M. Gerloch in *Transition Metal Chemistry*, VCH, Weinheim, **1994**.

[21] E. König, *Nature and Dynamics of the Spin-State Interconversion in Metal Complexes*, *Vol. 76*, Springer, Heidelberg, **1991**.

[22] R. L. Carlin, *Magnetochemistry*, 1st ed., Springer, Berlin, **1986**.

[23] G. M. Sheldrick, *Acta Crystallogr. Sect. A* **1990**, *46,* 467.

[24] G. M. Sheldrick, SHELXTL97–2; University of Göttingen, Göttingen, Germany, **1997**.

[25] G. S. Hanan, Ph. D. Thesis, Université Louis Pasteur, Strasbourg, **1995**.

[26] G. S. Hanan, U. S. Schubert, D. Volkmer, E. Riviére, J.-M. Lehn, N. Kyritsakas, J. Fischer, *Can. J. Chem.* **1997**, *75*, 169.

[27] J. Rojo, F. J. Romero-Salguero, J.-M. Lehn, G. Baum, D. Fenske, *Eur. J. Inorg. Chem.* **1999**, 1421–1428.

[28] E. Breuning, U. Ziener, J.-M. Lehn, E. Wegelius, K. Rissanen, *Eur. J. Inorg. Chem.* **2001**, 1515- 1521.

Received: March 6, 2003 [F4933]

